
**FRIEDRICH-ALEXANDER-UNIVERSITY**
**ERLANGEN-NÜRNBERG**
FACULTY OF ENGINEERING
DEPARTMENT OF COMPUTER SCIENCE

**Chair for Computer Science 10**
**(System simulation)**

# Implementation of Gaussian Schell beams into a Raytracing Framework

Jens Edel

Bachelor's Thesis

# Implementation of Gaussian Schell beams into a Raytracing Framework

Jens Edel

Bachelor's Thesis

| | |
|---|---|
| 1st Supervisor: | Prof. Dr. Christoph Pflaum |
| 2nd Supervisor: | M. Sc. Phillip Rall |
| Bearbeitungszeitraum: | 14.11.2020 – 22.07.2021 |

**Erklärung:**

Ich versichere, dass ich die Arbeit ohne fremde Hilfe und ohne Benutzung anderer als der angegebenen Quellen angefertigt habe und dass die Arbeit in gleicher oder ähnlicher Form noch keiner anderen Prüfungsbehörde vorgelegen hat und von dieser als Teil einer Prüfungsleistung angenommen wurde. Alle Ausführungen, die wörtlich oder sinngemäß übernommen wurden, sind als solche gekennzeichnet.

Der Universität Erlangen-Nürnberg, vertreten durch den Lehrstuhl für Systemsimulation (Informatik 10), wird für Zwecke der Forschung und Lehre ein einfaches, kostenloses, zeitlich und örtlich unbeschränktes Nutzungsrecht an den Arbeitsergebnissen der einschließlich etwaiger Schutzrechte und Urheberrechte eingeräumt.

Erlangen, den 29. Juli 2021 .....

# Table of Contents


1 Introduction . . . 2
1.1 The eikonal equation . . . 2
1.2 Limitations of the eikonal equation . . . 4
1.3 Solutions of the eikonal equation . . . 5
2 Coherence . . . 6
2.1 Mathematical Description of Coherence . . . 7
2.2 Wigner Distribution Function . . . 8
2.3 Moments of the Wigner Distribution Function . . . 9
3 Gaussian Schell Beams . . . 10
3.1 Mathematical descriptions for Gaussian Schell beams . . . 11
3.2 Characterization of general partially coherent beams . . . 13
4 Implementation into a raytracing framework . . . 14
4.1 Generating Wigner distributed rays . . . 15
4.2 Wigner moments and beam quality . . . 16
4.3 Limitations of the Wigner distribution function . . . 17
4.4 Evaluation . . . 17
5 Conclusion . . . 18

**Abstract.** Raytracing is an important technique used in many modern day applications ranging from photorealistic image simulation to physically tracing a ray through arbitrary optical systems. The major goal of this thesis is to implement partially coherent Gaussian Schell modelled beams into an existing raytracing framework. Based on the fundamentals of raytracing and the coherence of light, mathematical descriptions of these concepts are introduced and used for the derivation of the Wigner distribution function for Gaussian Schell modelled beams. The Wigner distribution function is utilized for the calculation of the beam quality. A bidimensional and tridimensional approach to the computation of the beam quality is derived from the moments of the Wigner distribution function which are measures of the extents of a beam. Finally, the basic structure of the algorithm is laid out and an evaluation of the model is presented.

# 1 Introduction

The book on Principles of optics by Max Born and Emil Wolf [4] is the underlying source of this chapter and will not repeatedly be cited.
Raytracing is classified by two major sections, one being related to computer graphics and the other to physics. The first is a rendering technique in which the path of light is traced as pixels in an image plane and optical effects like refraction or diffraction are simulated to create highly realistic images. The idea dates back to the 16th century as the German artist Albrecht Dürer described an apparatus called the *Dürer's Door* which essentially uses threads in order to trace rays from an object to find the contours to draw[3]. On the other hand, raytracing in physics is a subject where the path of waves and particles through any arbitrary system can be mathematically modelled and calculated. The most straightforward application is found in lasers since they emit highly monochromatic light on short wavelengths. As a particularly collimated beam, most light is focussed into one direction meaning that splitting the main beam into seperate partial beams is relatively simple. The simulation of such system opens up new possibilities to analyzing the properties of light such as the beam quality, where higher quality may lead to a higher laser output power required for industry applications[2]. Raytracing is part of geometrical optics which functions as the limiting case of wave optics for smaller wavelengths $\lambda \to 0$ implying that large wavelengths in the infrared spectrum can generally not be modeled while gamma radiation can rather easily be implemented.

## 1.1 The eikonal equation

Universally speaking, light can be described as an electromagnetic wave, meaning the Maxwell equations may be used to attain the basic equations of geometrical optics. Since Maxwells equations are a general description of optical fields, the medium in which the light propagates has to be restricted to be only linear and isotropic and its electric charge density $\rho$ has to be set to zero [4]. Following these limitations the Maxwells equations are reduced to

$$\nabla \times E = -\frac{\partial B}{\partial t} \qquad \text{(Ampères Law)} \quad (1.1.1)$$

$$\nabla \times H = \frac{\partial D}{\partial t} \qquad \text{(Faradays Law)} \quad (1.1.2)$$

$$\nabla \cdot D = 0 \qquad \text{(Coulombs Law)} \quad (1.1.3)$$

$$\nabla \cdot B = 0 \qquad \text{(Gaussian Law)} \quad (1.1.4)$$

while the meaning of each equation is clear:
Eq. (1.1.1): The change of magnetic induction $\boldsymbol{B}$ creates vortexes of the electric field $\boldsymbol{E}$.
Eq. (1.1.2): The rotation of the magnetic field $\boldsymbol{H}$ is caused only by a temporal variation of the electric displacement $\boldsymbol{D}$.
Eq. (1.1.3): Usually the sources of displacement $\boldsymbol{D}$ are the electric charges with density $\rho$ but since the limiting case for geometrical optics omits this, no electric charges exist.
Eq. (1.1.4): Similar to the gaussian law the magnetic field is solenoidal and therefore no magnetic charges exist.
The Nabla operator $\nabla$ is defined as

$$\nabla = \begin{pmatrix} \frac{\partial}{\partial x} \\ \frac{\partial}{\partial y} \\ \frac{\partial}{\partial z} \end{pmatrix} \quad (1.1.5)$$

and the vector product $\nabla \times \boldsymbol{f} = rot\boldsymbol{f}$ represents the curl of $\boldsymbol{f}$ and the scalar product $\nabla \cdot \boldsymbol{f} = div\boldsymbol{f}$ the divergence of $\boldsymbol{f}$ while in future functions $\nabla\varphi = grad\varphi$ is the gradient of a scalar function $\varphi$. Furthermore, $\boldsymbol{B}, \boldsymbol{D}, \boldsymbol{E}$ and $\boldsymbol{H}$ in the case of linear and isotropic materials are defined by

$$\boldsymbol{D}(\boldsymbol{r},t) = \epsilon(\boldsymbol{r})\epsilon_0\boldsymbol{E}(\boldsymbol{r},t) \quad (1.1.6) \qquad \boldsymbol{E}(\boldsymbol{r},t) = e(\boldsymbol{r})e^{ik_0L(\boldsymbol{r})}e^{-i\omega t} \quad (1.1.8)$$

$$\boldsymbol{B}(\boldsymbol{r},t) = \mu(\boldsymbol{r})\mu_0\boldsymbol{H}(\boldsymbol{r},t) \quad (1.1.7) \qquad \boldsymbol{H}(\boldsymbol{r},t) = h(\boldsymbol{r})e^{ik_0L(\boldsymbol{r})}e^{-i\omega t} \quad (1.1.9)$$

whereas $\epsilon(\boldsymbol{r})$ denotes the dielectric function and $\mu(\boldsymbol{r})$ the magnetic permeability, both as a function of the position $\boldsymbol{r}$. Meanwhile, $\epsilon_0$ and $\mu_0$ are the dielectric constant of vacuum and the constant magnetic permeability of vacuum. The real function $L$ is the optical path length while $e$ and $h$ represent the appropriate polarization states for the position $r$. It is worth noting that Eq. (1.1.8) and Eq. (1.1.9) are described by a general approach for stationary monochromatic waves. Putting these into Maxwells equations will yield the time-independent Maxwell equations:

$$\nabla \times (\boldsymbol{e}(\boldsymbol{r})e^{ik_0L(\boldsymbol{r})}) = i\omega\mu(\boldsymbol{r})\mu_0\boldsymbol{h}(\boldsymbol{r})e^{ik_0L(\boldsymbol{r})} \quad (1.1.10) \qquad \nabla \cdot (\mu(\boldsymbol{r})\mu_0\boldsymbol{h}(\boldsymbol{r}))e^{ik_0L(\boldsymbol{r})}) = 0 \quad (1.1.12)$$

$$\nabla \times (\boldsymbol{h}(\boldsymbol{r})e^{ik_0L(\boldsymbol{r})}) = i\omega\epsilon(\boldsymbol{r})\epsilon_0\boldsymbol{e}(\boldsymbol{r})e^{ik_0L(\boldsymbol{r})} \quad (1.1.11) \qquad \nabla \cdot (\epsilon(\boldsymbol{r}\epsilon_0\boldsymbol{e}(\boldsymbol{r}))e^{ik_0L(\boldsymbol{r})}) = 0 \quad (1.1.13)$$

The nabla calculus $\nabla \cdot (\nabla \times \boldsymbol{f}) = 0$, where $\boldsymbol{f}$ is any arbitrary vector function, will be applied to the right hand side of Eq. (1.1.10) and Eq. (1.1.11) resulting in:

$$\begin{aligned}\nabla \times (\boldsymbol{e}(\boldsymbol{r})e^{ik_0L(\boldsymbol{r})}) &= \nabla(e^{ik_0L(\boldsymbol{r})})) \times \boldsymbol{e}(\boldsymbol{r}) + e^{ik_0L(\boldsymbol{r})})\nabla \times \boldsymbol{e}(\boldsymbol{r}) \\ &= [ik_0\nabla L(\boldsymbol{r}) \times \boldsymbol{e}(\boldsymbol{r}) + \nabla \times \boldsymbol{e}(\boldsymbol{r})]e^{ik_0L(\boldsymbol{r})}\end{aligned} \quad (1.1.14)$$

$$\nabla \times (\boldsymbol{h}(\boldsymbol{r})e^{ik_0L(\boldsymbol{r})}) = [ik_0\nabla L(\boldsymbol{r}) \times \boldsymbol{h}(\boldsymbol{r}) + \nabla \times \boldsymbol{h}(\boldsymbol{r})]e^{ik_0L(\boldsymbol{r})} \quad (1.1.15)$$

These can be reduced to

$$\nabla L(\boldsymbol{r}) \times (\boldsymbol{e}(\boldsymbol{r}) - c\mu(\boldsymbol{r})\mu_0\boldsymbol{h}(\boldsymbol{r}) = \frac{i}{k_0}\nabla \times \boldsymbol{e}(\boldsymbol{r}) \quad (1.1.16)$$

$$\nabla L(\boldsymbol{r}) \times (\boldsymbol{h}(\boldsymbol{r}) + c\epsilon(\boldsymbol{r})\epsilon_0\boldsymbol{e}(\boldsymbol{r}) = \frac{i}{k_0}[\nabla \times \boldsymbol{h}(\boldsymbol{r})] \quad (1.1.17)$$

and under consideration of $\lambda \to 0$ ($k_0 = \frac{2\pi}{\lambda} \overset{\lambda \to 0}{=} \infty$) the right sides vanish:

$$\nabla L(\boldsymbol{r}) \times (\boldsymbol{e}(\boldsymbol{r}) - c\mu(\boldsymbol{r})\mu_0\boldsymbol{h}(\boldsymbol{r}) = 0 \quad (1.1.18)$$

$$\nabla L(\boldsymbol{r}) \times (\boldsymbol{h}(\boldsymbol{r}) + c\epsilon(\boldsymbol{r})\epsilon_0\boldsymbol{e}(\boldsymbol{r}) = 0 \quad (1.1.19)$$

By solving Eq. (1.1.18) for $\boldsymbol{h}(\boldsymbol{r})$ and pushing the result into Eq. (1.1.19), the formula takes the following form:

$$\begin{aligned}&\frac{1}{c\mu(\boldsymbol{r}\boldsymbol{\mu_0})}\nabla L(\boldsymbol{r}) \times (L(\boldsymbol{r}) \times \boldsymbol{e}(\boldsymbol{r})) + c\epsilon(\boldsymbol{r})\epsilon_0\boldsymbol{e}(\boldsymbol{r}) = 0 \\ \Rightarrow\ &(\nabla L(\boldsymbol{r}) \cdot \boldsymbol{e}(\boldsymbol{r}))\nabla L(\boldsymbol{r}) - (\nabla L(\boldsymbol{r}))^2\boldsymbol{e}(\boldsymbol{r}) + n^2(\boldsymbol{r})\boldsymbol{e}(\boldsymbol{r}) = 0\end{aligned} \quad (1.1.20)$$

The relations $\mu_0\epsilon_0 = \frac{1}{c^2}$ and $\mu\epsilon = n^2$ introduce the refractive index $n$ and are implemented to shorten the expressions. Finally, the eikonal equation can be stated by utilizing $\nabla L \cdot e = 0$ in Eq. (1.1.19):

$$(\nabla L(\boldsymbol{r}))^2 = n^2(\boldsymbol{r}) \quad (1.1.21)$$

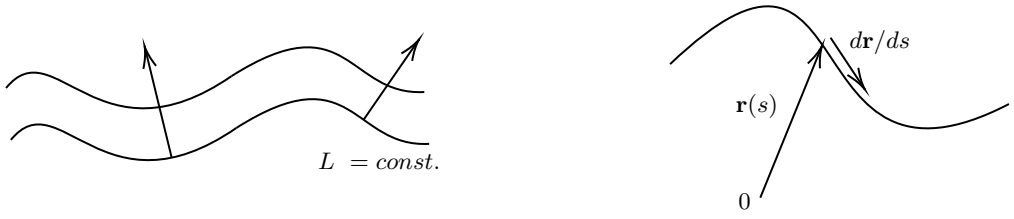


(a) (b)

Fig. 1: a) The optical ray is the trajectory which is perpendicular to the surfaces of equal optical path length $L$, b) An arbitrary light ray where $\boldsymbol{r}(s)$ is the position vector of a point on the ray and $s$ the arc length along the curve and 0 the origin of the coordinate system [4]

The eikonal equation is the basic equation in geometrical optics and is a fundamental notation for the expression of optical rays in physics. Such ray is used to model the propagation of light where the propagation direction is always perpendicular to the wave fronts which are the surfaces of the optical path length $L$ (see Fig. 1a). If a surface with constant $L$ is considered, a ray points into a certain direction starting from any point in space while being perpendicular to the surfaces of equal optical path length $\nabla L$. From the fact that $\nabla L$ points into the same direction as the ray, the ray equation in Eq. (1.1.22) is established. Compared to Eq. (1.1.21) $\boldsymbol{r}$ is now the position vector and $\frac{d\boldsymbol{r}}{ds}$ the unit vector tangential to the ray curve (see Fig. 1b). Furthermore, $L(\boldsymbol{r})$ and $n(\boldsymbol{r})$ are now referred to as $L$ and $n$ to simplify future notations.

$$\nabla L = n\frac{d\boldsymbol{r}}{ds} \tag{1.1.22}$$

The differential equation for a ray can be derived from Eq. (1.1.22) by using $\frac{d}{ds}\nabla L$ as the directional derivative of $\nabla L$ along the rays direction $\frac{d\boldsymbol{r}}{ds}$ and then utlizing $n^2 = \mu\epsilon$ and Eq. (1.1.21) to achieve the final equation:

$$\begin{aligned} \frac{d}{ds}\left(n\frac{d\boldsymbol{r}}{ds}\right) = \frac{d}{ds}\nabla L(\boldsymbol{r}) = \frac{d\boldsymbol{r}}{ds}\cdot\nabla(\nabla L) \\ = \frac{1}{n}\nabla L\cdot\nabla(\nabla L) = \frac{1}{2n}\nabla(\nabla L)^2 = \frac{1}{2n}\nabla n^2 = \nabla n \\ \Rightarrow \frac{d}{ds}(n\frac{d\boldsymbol{r}}{ds}) = \nabla n \end{aligned} \tag{1.1.23}$$

## 1.2 Limitations of the eikonal equation

Because Eq. (1.3.3) only is relevant for raytracing in open spaces where the refractive index $n$ is constant, a different approach is necessary for gradient mediums. The scalar Helmholtz equation with wave field $u(\boldsymbol{r})$ may be utilized for this approach:

$$\nabla^2 u(\boldsymbol{r}) - \frac{1}{c^2}\frac{\delta^2 u(\boldsymbol{r})}{\delta t^2} = [\nabla^2 + (nk_0)^2]u(\boldsymbol{r}) = 0 \tag{1.2.1}$$

The wave function $u$ is defined as

$$u(\boldsymbol{r}) = A(\boldsymbol{r})e^{ik_0 L(\boldsymbol{r})} \tag{1.2.2}$$

while $A$ is the amplitude of the wave. The gadient of $u$ can be modified to

$$\begin{aligned}\nabla u &= \nabla\left[Ae^{ik_0L}\right] = e^{ik_0L}\nabla A + ik_0Ae^{ik_0L}\nabla L \\ &= \Big(\frac{\nabla A}{A} + ik_0\nabla L\Big)u\end{aligned} \tag{1.2.3}$$

and the Laplacian of $u$ to:

$$\begin{aligned}\Delta u &= \Big(\frac{\nabla A}{A} + ik_0\nabla L\Big)u \\ &= \Big(\frac{\nabla A}{A} + ik_0\nabla L\Big)^2 u + \Big(\frac{\Delta A}{A} + \frac{(\nabla A)^2}{A^2} + ik_0\Delta L\Big)u \\ &= \Big(\frac{\Delta A}{A} - k_0^2(\nabla L)^2 + 2ik_0\frac{\nabla A\cdot\nabla L}{A} + ik_0\Delta L\Big)u\end{aligned} \tag{1.2.4}$$

$\Delta = \nabla\cdot\nabla$ is called the Laplace operator or Laplacian. This is inserted into Eq. (1.2.1) and then divided by $u$ to shorten it to:

$$\frac{\Delta A}{A} - k_0^2(\nabla L)^2 + n^2k_0^2 + 2ik_0\frac{\nabla A\cdot\nabla L}{A} + ik_0\Delta L = 0 \tag{1.2.5}$$

For slowly changing directions and outside the limiting case of $\lambda\to 0$, the real part of the eikonal equation is given by

$$\begin{aligned}&\frac{\Delta A}{A} - k_0^2(\nabla L)^2 + n^2k_0^2 = 0 \\ &\Rightarrow (\nabla L)^2 = n^2 + \frac{1}{k_0^2}\frac{\Delta A}{A} = n^2 + \gamma\end{aligned} \tag{1.2.6}$$

It is worth noting that $\gamma$ has to be small, i.e. either $\lambda$ or $\Delta A$ has to be smaller than $n^2$, which in most cases in the geometrical zone, far away from diffraction zones, is true.

### 1.3 Solutions of the eikonal equation

In inhomogenous isotropic and linear materials, the refractive index is dependant on the position. Even though the solution for such materials can be very complex it is not a big problem because in most relevant cases homogenous materials are used. With this simplification the differential equation is reduced to

$$\frac{d^2\boldsymbol{r}}{ds^2} = 0 \tag{1.3.1}$$

and can relatively easy be solved by a straight line. The ray equation in homogenous materials therefore is

$$\boldsymbol{r} = s\boldsymbol{a} + \boldsymbol{p} \tag{1.3.2}$$

with $\boldsymbol{a}$ and $\boldsymbol{p}$ as constant vectors. More precisely, because $s$ is the geometrical path length, $\boldsymbol{a}$ has to be a unit vector along the ray indicating that $s_2 > s_1$ for two points $P_1$ and $P_2$ and the position vectors $\boldsymbol{r_1}$ and $\boldsymbol{r_2}$:

$$|\boldsymbol{r_2} - \boldsymbol{r_1}| = (s_2 - s_1)|\boldsymbol{a}| = s_2 - s_1 \Rightarrow |\boldsymbol{a}| = 1 \tag{1.3.3}$$

For optical systems in which the refractive index changes, the direction vector $\boldsymbol{a}$ is split into the vectors $\boldsymbol{a}_1$ and $\boldsymbol{a}_2$. $\boldsymbol{a}_1$ points in the direction of the surface where the refractive index changes

($n_1 \to n_2$, for example at a lens), while $\boldsymbol{a}_2$ represents the refracted ray. If the incident ray $\boldsymbol{a}_1$, the local surface normal $N$ and the two refractive indices $n_1$ and $n_2$ are known, the following equation for the the direction vector $\boldsymbol{a}_2$ is applicable:

$$\boldsymbol{a}_2 = \frac{n_1}{n_2}\boldsymbol{a}_1 - \frac{n_1}{n_2}(\boldsymbol{a}_1 \cdot \boldsymbol{N})\boldsymbol{N} \pm \boldsymbol{N}\sqrt{1 - \left(\frac{n_1}{n_2}\right)^2 [1 - (\boldsymbol{a}_1 \cdot \boldsymbol{N})^2]} \tag{1.3.4}$$

## 2 Coherence

If not explicitly stated this chapters and its subchapters content is based on [7].
Light can be categorized by various properties like its intensity, direction of propagation, frequency, wavelength, polarization and the speed of light. At optical frequencies of order $1 \times 10^{14}$ Hz, the intensity of light is usually the only property that can be measured. Nevertheless it is possible to derive the absolute value of the amplitude of the elctrical field by using the measured intensity. Additionally, the effect of interference may be used for relative measurements like the optical path length or optical image formation and may also indicate the observability of interference effetcts. Coherence shows to which degree two seperate beams of light can interfere, meaning two completely incoherent beams cannot interfere with each other and coherent beams may display an intereference pattern. As lasers provide a highly coherent source of light they often suffer from undesired interference, e.g. by scattering at rough surfaces, atmospheric turbulences or contaminations, know as speckle effects[7].
Coherence in general describes to what degree the phases of the complex field components are coupled. Incoherent light results in reduced contrast of the interference pattern of interfering light waves and phase changes have a small impact on changing it. In reverse, the resulting pattern for coherent light is highly contrasted and sensitive to phase changes as all phases are coupled. Lasers resemble coherent light sources since the phases of light waves inside a resonator need to be aligned in order for the Laser to be operating. Therefore coherent wave fields can be described by single modes and incoherent wave fields as multiple independent modes[7].
Since light is dependent on time and space, it is intuitive that coherence is a spatial-temporal phenomenon. For temporal coherence, a wave is compared to a delayed part of itself, meaning it is observed at the same place at different points in time. In order to visualize temporal coherence, a Michelson interferometer can be used to split a beam into two seperate waves and delay one of them[4]. When recombining at a screen, an interference pattern will become detectable if the source light is coherent. Temporal coherence not only characterizes how well a wave can interfere with its delayed counterpart, but is also used as a measure of how monochromatic light is. Spatial coherence however is the cross-correlation between two points of a wave at any time and describes to which degree waves at two different points in space can interfere. By geometrically splitting a wave, using Young's double-slit interferometer, it is possible to observe spatial coherence. Spatial coherence also may be referred to the visibility when spatially shifted waves recombine. In order to distinguish fields with different spatial coherence the Wigner space is used. At each point in a coherent field exists a strong coherent field strength and thus may interfere everywhere. The Wigner distribution function can be used in such space and by showing negative values diffraction and interference effects are measurable[7].

### 2.1 Mathematical Description of Coherence

Coherence can mathematically be modelled by the coherence function $\Gamma$ which is stated as the correlation of the complex field amplitudes at different points in space and time

$$\begin{aligned}\Gamma_{12} = \Gamma(\boldsymbol{r_1}, \boldsymbol{r_2}, \tau) &= \langle U(\boldsymbol{r_1}, t+\tau) U^*(\boldsymbol{r_2}, t)\rangle_\tau \\ &= \frac{1}{\tau}\int_t^{t+\tau} U(\boldsymbol{r_1}, t+\tau)\cdot U^*(\boldsymbol{r_2}, t)\, dt.\end{aligned} \tag{2.1.1}$$

In this definition of $\Gamma$, the light originates from the same source meaning the cross-correlation is given at different times $t$ and locations $r$ in the same field. In general the complex representation of $U_n$ ($n^{th}$ wave) is considered as

$$U_n = A_n e^{i(k_n r - \omega_n t + \varphi_n)}. \tag{2.1.2}$$

Inserting $U$ into the $\Gamma$-function, results in the first-order mutual coherence function, which shows the correlation of two signals $U_1$ and $U_2$ at the same position $\boldsymbol{r}$

$$\begin{aligned}\Gamma(U_n, U_m) = \langle |U_n U_m^*| \rangle_\tau &= \frac{1}{\tau}\int_0^\tau U(\boldsymbol{r}, t+\tau)\cdot U^*(\boldsymbol{r}, t)\, dt \\ &= \frac{1}{\tau}\int_0^\tau A_n e^{i(k_n r - \omega_n(t+\tau)+\varphi_1)} \cdot A_m e^{-i(k_m r - \omega_m t + \varphi_2)}\, dt \\ &= \frac{1}{\tau}\int_0^\tau A_n A_m \cdot cos[\Delta k_{nm} r - \omega_n(t+\tau) + \omega_m t + \varphi_{nm}]\, dt\end{aligned} \tag{2.1.3}$$

$$\Delta k_{nm} = k_n - k_m, \qquad \Delta\varphi_{nm} = \varphi_n - \varphi_m. \tag{2.1.4}$$

For $n = m$ the function corresponds to the normal or mutual intensity. In this way the $\Gamma$-function can be used in order to calculate the intensity while same positions $\boldsymbol{r_1} = \boldsymbol{r_2} = \boldsymbol{r}$ and same points in time are considered. The sum of the coherence functions from all individual wave fields leads to obtaining the total intensity of the observed light:

$$I(r,t) = \sum_{n,m}\Gamma(U_n, U_m) = \sum_{n,m}\sqrt{I_n I_m}\gamma(U_n, U_m) \tag{2.1.5}$$

Since it is a mathematical construction, the coherence function cannot directly be measured and therefore has to be evalutated in another way. This is done by the complex degree of coherence $\gamma$ which is calculated by normalizing the coherence function and thus is limited by $0 \leq |\gamma| \leq 1$:

$$\gamma_{12}(\tau) = \gamma(\boldsymbol{r_1}, \boldsymbol{r_2}, \tau) = \frac{\Gamma_{12}(\tau)}{\sqrt{\Gamma_{11}(0)\cdot\Gamma_{22}(0)}} = \frac{\Gamma(\boldsymbol{r_1}, \boldsymbol{r_2}, \tau)}{\sqrt{I(\boldsymbol{r_1})\cdot I(\boldsymbol{r_2})}} \tag{2.1.6}$$

$$\begin{aligned}I(\boldsymbol{r}) &= I_1(\boldsymbol{r}) + I_2(\boldsymbol{r}) + 2A_1A_2 cos(\Delta k\cdot r + \Delta\varphi) \\ &= I_1(\boldsymbol{r}) + I_2(\boldsymbol{r}) + 2\Gamma(\boldsymbol{r_1}, \boldsymbol{r_2}, 0) \\ &= I_1(\boldsymbol{r}) + I_2(\boldsymbol{r}) + 2\gamma_{12}(0)\cdot\sqrt{I_1(\boldsymbol{r})I_2(\boldsymbol{r})}\end{aligned} \tag{2.1.7}$$

A strong correlation between the seperate light sources, e.g. a higher degree of coherence, leads to a higher contrast of the interference pattern. The standard equation for the visibility $V$ can now be expressed by using $\gamma$:

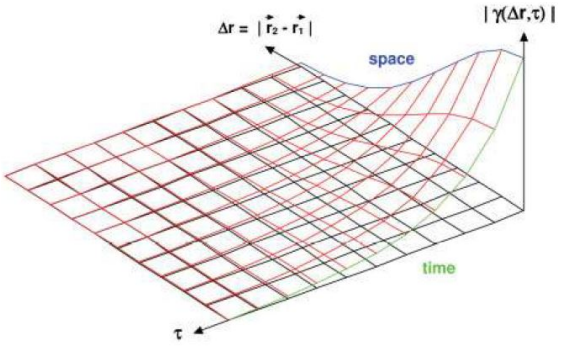


Fig. 2: Plot of the decreasing degree of coherence while $\Delta r$ and $\tau$ increase [7]

As seen in Fig. 2 $\gamma$ decreases depending on the distance $\Delta r$ between two wave fields and their time difference $\tau$. As the spatial and temporal difference decreases the degree of coherence increases until the two wave fields are at the exact same point in space and time and perfect coherence is achieved. In this special circumstance is the resulting coherence function is the cross-correlation of the same wave field.
The intensity of two point light sources can then be calculated using the time-independent form $I(\boldsymbol{r})$ and $\gamma_{12}(0)$

$$V = \frac{I_{max} - I_{min}}{I_{max} + I_{min}} = \frac{2\sqrt{I_1(\boldsymbol{r}) \cdot I_2(\boldsymbol{r})}}{I_1(\boldsymbol{r}) + I_2(\boldsymbol{r})} \cdot \gamma_{12}(0) \tag{2.1.8}$$

Using this notation can simplify the calculation of $V$ as for two source points and $\gamma = 0$ the visibility becomes 0 and no interference can be observed. The temporal Fourier transform of the coherence function, also called the cross-spectral density, is an important distribution when temporal coherence is considered:

$$S(\boldsymbol{r_1}, \boldsymbol{r_2}, \omega) = \int_{-\infty}^{\infty} \Gamma(\boldsymbol{r_1}, \boldsymbol{r_2}, t) \cdot e^{-i\omega t}\, dt \tag{2.1.9}$$

The propagation of an electromagnetic wave in vacuum is described by the Helmholtz formulation from Eq. (1.2.1) which is modified for the field amplitudes $U_1$ and $U_2$:

$$\nabla^2 U - \frac{1}{c^2}\frac{\delta^2 U}{\delta t^2} = 0 \tag{2.1.10}$$

## 2.2 Wigner Distribution Function

The Wigner distribution function allows the description of mechanical phenomena in a phase space. As the phase space is linked to geometrical optics where position and direction of optical rays are considered, an optical field modelled by rays can be represented by the Wigner distribution. Additionally, the Wigner distribution function $W$ is applicable for partially coherent light since it contains coherence properties for the propagation through optical systems.
By introducing the center of mass $r$ along with the transverse spatial frequency coordinate $\nu$ the coherence function can be expressed by

$$\Gamma(\boldsymbol{r_1}, \boldsymbol{r_2}) \rightarrow J(\boldsymbol{r}, \Delta\boldsymbol{r}) \tag{2.2.1}$$

$$\boldsymbol{r} = \frac{\boldsymbol{r_1} + \boldsymbol{r_2}}{2}, \quad \Delta\boldsymbol{r} = \boldsymbol{r_1} - \boldsymbol{r_2} \tag{2.2.2}$$

$$\boldsymbol{v} = \frac{\boldsymbol{v_1} + \boldsymbol{v_2}}{2}, \quad \Delta\boldsymbol{v} = \boldsymbol{v_1} - \boldsymbol{v_2} \tag{2.2.3}$$

Moreover, the spatial Fourier transform of $\Gamma$ is needed:

$$\bar{\Gamma}(\boldsymbol{v_1}, \boldsymbol{v_2}) = \int\int \Gamma(\boldsymbol{r_1}, \boldsymbol{r_2}) e^{-i2\pi(\boldsymbol{v_1 r_1} - \boldsymbol{v_2 r_2})}\, d\boldsymbol{r_1} d\boldsymbol{r_2} \tag{2.2.4}$$

The definition of the Wigner distribution function $W(\boldsymbol{r}, \boldsymbol{v})$ is then stated as

$$\begin{aligned} W(\boldsymbol{r}, \boldsymbol{v}) &= \int \Gamma\left(\boldsymbol{r} + \frac{\Delta \boldsymbol{r}}{2}, \boldsymbol{r} - \frac{\Delta \boldsymbol{r}}{2}\right) e^{-i2\pi \Delta \boldsymbol{r} \boldsymbol{v}} \, d\Delta \boldsymbol{r} \\ &= \int \bar{\Gamma}\left(\boldsymbol{v} + \frac{\Delta \boldsymbol{v}}{2}, \boldsymbol{v} - \frac{\Delta \boldsymbol{v}}{2}\right) e^{-i2\pi \Delta \boldsymbol{v} \boldsymbol{r}} \, d\Delta \boldsymbol{v} \end{aligned} \tag{2.2.5}$$

The second input parameter can be modified to represent the x- and y-components of the optical direction cosine vector $\boldsymbol{u}$ which is given by the angle $\alpha$ relative to the optical axis:

$$W'(\boldsymbol{r}, \boldsymbol{u}) = \int \Gamma\left(\boldsymbol{r} + \frac{\Delta \boldsymbol{r}}{2}, \boldsymbol{r} - \frac{\Delta \boldsymbol{r}}{2}\right) e^{-ik_0 \Delta \boldsymbol{r} \boldsymbol{u}} \, d\Delta \boldsymbol{r} \tag{2.2.6}$$

$$\boldsymbol{u} = sin\alpha = \lambda \boldsymbol{v} = \frac{\lambda}{2\pi} \cdot \boldsymbol{k} \tag{2.2.7}$$

This allows the Wigner distribution function $W'$ and the coherence function to contain the same information represented in different ways. It provides the amplitude of a beam at a position $(r_x, r_y)$ and direction $(u_x, u_y)$ and embodys either the local angular spectrum at position $\boldsymbol{r}$ or the local averaged phase space density. The Wigner distribution function takes effects like interference and diffraction into consideration while it also is suitable for coherent and incoherent radiation. Furthermore, the resulting values of $W'$ do not have to be positive, as negative values can show destructive interference and thus a decrease or even elimination of the intensity.

### 2.3 Moments of the Wigner Distribution Function

As previously stated, the Intensity can be obtained by using the Wigner distribution function $W'$. If integrated over $\boldsymbol{r}$ the direction spectrum of the intensity is obtained while integration over $\boldsymbol{u}$ gives the spatial distribution of the intensity:

$$I(\boldsymbol{u}) = \int W'(\boldsymbol{r}, \boldsymbol{u}) \, d\boldsymbol{r} \tag{2.3.1}$$

$$I(\boldsymbol{r}) = \int W'(\boldsymbol{r}, \boldsymbol{u}) \, d\boldsymbol{u} \tag{2.3.2}$$

Integration over $\boldsymbol{r}$ and $\boldsymbol{u}$ yields the total power of the entire field

$$P = \int \int W'(\boldsymbol{r}, \boldsymbol{u}) \, d\boldsymbol{r} d\boldsymbol{u} = \int I(\boldsymbol{r}) \, d\boldsymbol{r} \tag{2.3.3}$$

$P$ can further be used for the first- and second-order moments of the position and angle of the Wigner Function, indicating the extents or the shape of a beam accordingly.

$$\langle r_x \rangle = \int \int r_x \cdot W'(\boldsymbol{r}, \boldsymbol{u}) \, d\boldsymbol{r} d\boldsymbol{u} \tag{2.3.4}$$

$$\langle r_x^2 \rangle = \frac{1}{P} \int \int r_x^2 \cdot W'(\boldsymbol{r}, \boldsymbol{u}) \, d\boldsymbol{r} d\boldsymbol{u} = \frac{1}{P} \int r_x^2 I(\boldsymbol{r}) \, d\boldsymbol{r} \tag{2.3.5}$$

$$\langle u_x^2 \rangle = \frac{1}{P} \int \int u_x^2 \cdot W'(\boldsymbol{r}, \boldsymbol{u}) \, d\boldsymbol{r} d\boldsymbol{u} = \frac{1}{P} \int u_x^2 I(\boldsymbol{u}) \, d\boldsymbol{u} \tag{2.3.6}$$

$$\langle r_x r_y \rangle = \frac{1}{P} \int \int r_x r_y \cdot W'(\boldsymbol{r}, \boldsymbol{u}) \, d\boldsymbol{r} d\boldsymbol{u} \tag{2.3.7}$$

$$\langle r_x u_x \rangle = \frac{1}{P} \int \int r_x u_x \cdot W'(\boldsymbol{r}, \boldsymbol{u})\, d\boldsymbol{r} d\boldsymbol{u} \tag{2.3.8}$$

These higher order moments can help describe characteristics of lasers such as the beam quality.

## 3 Gaussian Schell Beams

The previously presented Wigner distribution function can be used to describe the coherence properties of a propagating wave field. It can help find a significantly more trivial application in paraxial systems, e.g. ray-tracing systems, and can be accomplished at a higher speed using numerical methods. A viable solution of the Wigner distribution function are Gaussian beams in the first approximation, the so-called Gaussian Schell beams. These are based on the elemental statistical assumptions of the coherence function $\Gamma$ and are used to model the propagation of partially coherent Gaussian beams.
For the Wigner distribution are following parameters of high importance:

Normalized transverse coherence length:

$$\alpha = \frac{L_c}{w_0} \tag{3.1}$$

Auxiliary parameter $\epsilon$:

$$\epsilon = 1 + \frac{1}{\alpha^2} = 1 + \left(\frac{w_0}{L_c}\right)^2 > 1 \tag{3.2}$$

Degree of coherence $\beta$:

$$\beta = \frac{1}{\sqrt{1 + (w_0/L_c)^2}} = \frac{1}{1 + \alpha^{-2}} = \frac{1}{\sqrt{\epsilon}} < 1 \tag{3.3}$$

The transverse coherence length $L_c$ is closely related to the degree of coherence. $w_0$ is the radius of the beam waist. For an infinite coherence length $L_c \to \infty$ the Gaussian Schell beams are perfectly coherent. A decreasing coherence length leads to more incoherent radiation, an increased beam divergence and thus a decreasing depth focus and a larger beam parameter product denoting a worse beam quality.
Analogous to the degree of coherence $\gamma$ for non Gaussian Schell beams, a perfectly coherent Gaussian Schell beam features $\beta = 1$ and $\beta = 0$ for a completely incoherent one. Figure Fig. 3a shows a plot of the Degree of coherence $\beta$. While this plot visualizes the fast decrease in coherence, a high value for $\beta$ is easily achieved when the use of lasers is taken into account. A standard multimode helium-neon laser exhibits a typical coherence length of $L_c = 20\,\mathrm{cm}$[6]. If the beam waist is at a very large $w_0 = 20\,\mathrm{cm}$, a degree of coherence as high as 70% is easily attained. For single-mode lasers the coherence length can exceed 100 m or even 100 km in fiber lasers resulting in an excellent $\beta = 99.99\%$. The graph in Fig. 3a visualizes the fast increase of the degree of coherence while Fig. 3b connects a high degree of coherence to the depth focus $z_0'/z_0 = \sqrt{\epsilon}$. A highly coherent wave field directly leads to stronger depth focus and thus higher contrast in the potential interference.

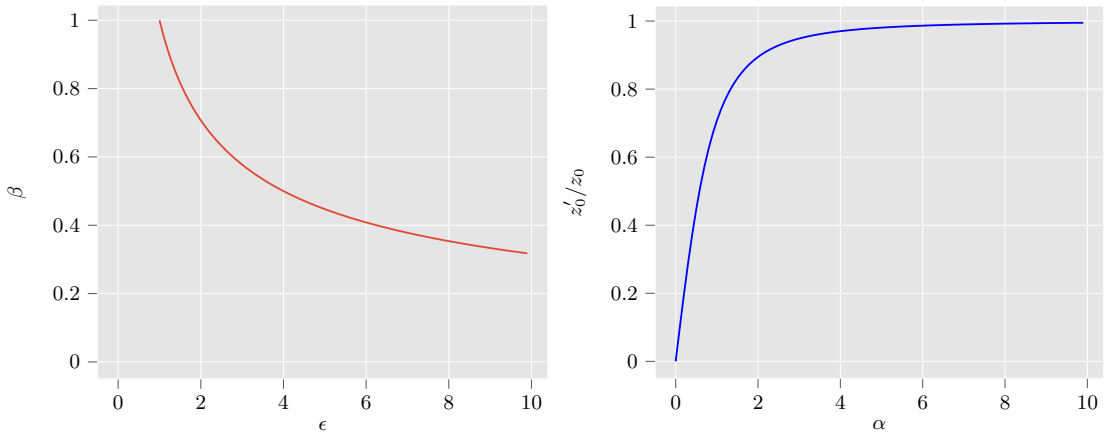


(a) (b)

Fig. 3: a) Degree of coherence $\beta$ and b) Depth focus as a function of the normalized transverse coherence length

In addition to the degree of coherence, the following equation denotes the coherence length at the position of the beam waist. Here at $z = 0$ the normalized degree of coherence $\beta(z)$ is constant and the auxiliary parameter $\epsilon$ is used to scale the far-field divergence angle $\theta_0$.

$$L_c = \frac{w_0}{\sqrt{\left(\frac{\pi w_0 \theta_0'}{\lambda}\right)^2 - 1}} \tag{3.4}$$

$$\beta(z) = const. \tag{3.5}$$

$$\theta_0' = \theta_0 \cdot \sqrt{\epsilon} \tag{3.6}$$

### 3.1 Mathematical descriptions for Gaussian Schell beams

In Sect. 2.1 the coherence function and wigner distribution for general light fields have been declared. Following the previous chapter, these funtions can be simplified using the presented Gaussian Schell model. The coherence function $\Gamma$ is now appointed by

$$\Gamma(\boldsymbol{r_1}, \boldsymbol{r_2}, z) = I_0 \cdot \left[\frac{w_0}{w(z)}\right]^2 e^{-\frac{\boldsymbol{r_1}^2+\boldsymbol{r_2}^2}{w^2(z)}} e^{-\frac{(\boldsymbol{r_1}-\boldsymbol{r_2})^2}{2L_c^2(z)}} e^{-\frac{i\pi(\boldsymbol{r_1}^2-\boldsymbol{r_2}^2)}{\lambda R(z)}} \tag{3.1.1}$$

The Wigner distribution function for partially coherent Gaussian Schell beams in paraxial approximation and at any point $z$ is now provided by

$$\begin{aligned} W(\boldsymbol{r}, \boldsymbol{u}) &= \frac{I_0}{2\pi} \cdot \frac{w^2(z) \cdot L_c^2(z)}{w^2(z) + L_c^2(z)} \cdot e^{-\frac{2\boldsymbol{r}^2}{w^2(z)}} \cdot e^{-\frac{2\pi^2}{\lambda^2} \frac{w^2(z) \cdot L_c^2(z)}{w^2(z)+L_c^2(z)} \cdot (\boldsymbol{u} - \frac{\boldsymbol{r}}{R})^2} \\ &= \frac{I_0}{2\pi} \cdot \frac{w^2(z) \cdot L_c^2(z)}{w^2(z) + L_c^2(z)} \cdot e^{-\frac{2\boldsymbol{r}^2}{w^2(z)}} \cdot e^{-\frac{2}{\theta^2}(\frac{\boldsymbol{r}}{R})^2} \end{aligned} \tag{3.1.2}$$

where $R(z)$ describes the radius of the wave front and $w(z)$ the beam radius, both at position $z$ along the beams direction of propagation. Besides representing the optical field and the general

phase-space as a ray, the Wigner distribution function is closely related to the intensity distribution in the current position $\boldsymbol{r}$ and its direction $\boldsymbol{u}$. The intensity distributions of Gaussian Schell Beams are shaped like a Gaussian bell both as a function of the transverse dimension $I(\boldsymbol{r})$ and of the angle $I(\boldsymbol{u})$. It is important to note that the graphs f) - i) in Fig. 4 are not accurate for the intensity distribution shown in the first row (from [7]) and solely serve as a visualization.
In Fig. 4, a single ray of a Gaussian Schell beam is propagated through a lens until it hits a screen. The leftmost vertical line in Fig. 4a represents the starting plane from Fig. 4b. The beams intensity is equally distributed and mostly collimated while being slightly divergent. The closer the plane of observation is to the lens, the more divergent the beam becomes and thus the larger the relative geometrical-optical angular contribution. The rotation in the phase space (seen in

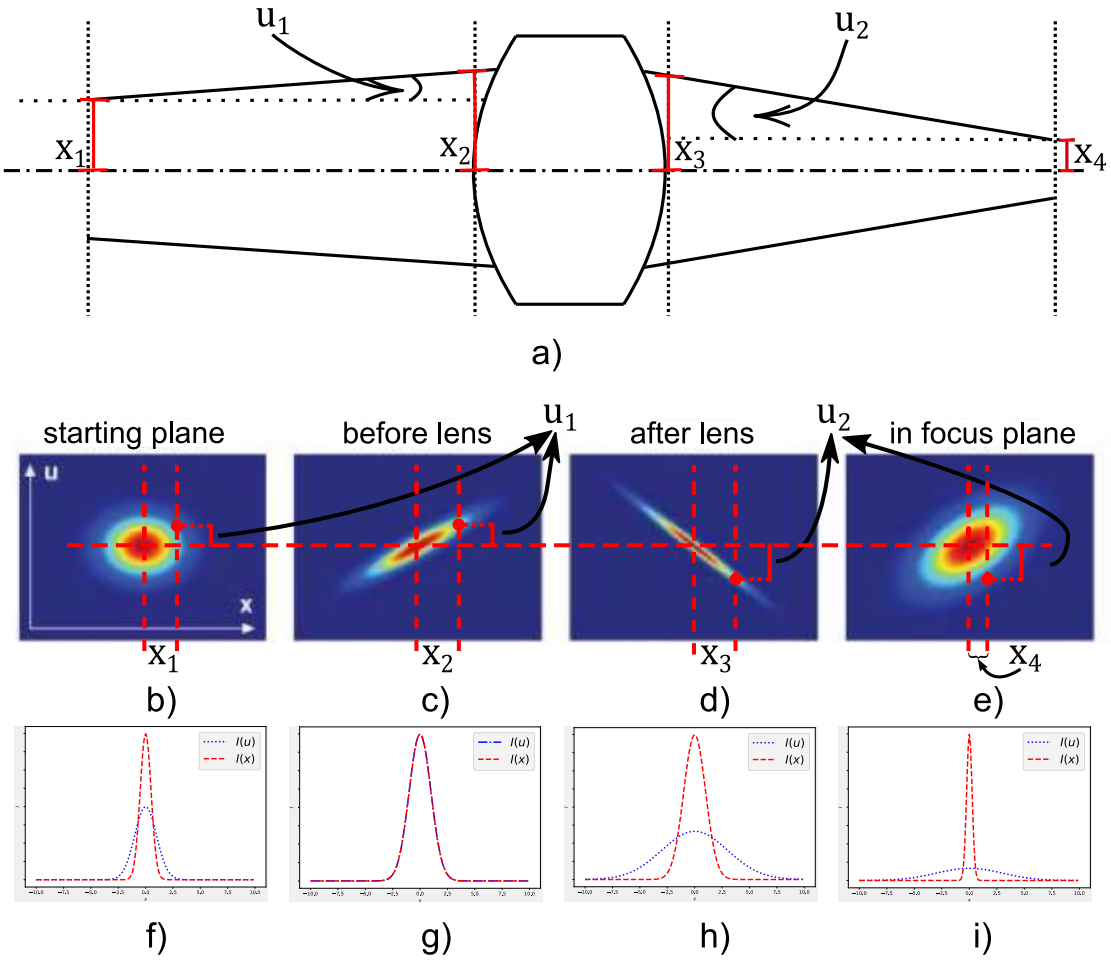


Fig. 4: a) Sketch of an optical system containing a convex lens, where a Gaussian Schell beam is propagated through. A single ray (position in the phase space marked in red) is more closely inspected with help of the four planes of observation $x_{1-4}$ and the angular shift $u_{1/2}$. b) - e) Intensity distributions of Gaussian Schell beams transformed by an ideal lens. The red lines demonstrate how a single ray contributes to the phase space by its change in position ($x_{1-4}$) and angle ($u_{1/2}$). f) - i) show the angular and spatial distributions $I(u)$ and $I(x)$. [7]

Fig. 4c and Fig. 4d) is related to the angular shift in Fig. 4a where the beam transitions from diverging to being focussed. While the spatial intensity distribution stays relatively constant, the angular intensity distribution now is significantly more flattend than before. The angle $u$ increases the further away the observed ray is from the center of the beam meaning a ray at the border of a beam has a higher divergence than a ray at the center. This effect intesifies as the beam propagates through the lens and beyond. The increasing angular contribution is shown by $u_1$ and $u_2$ whereas in the case of a diverging lens $u_1 > u_2$.
The Wigner function comes in handy as it can be used in the same manner after the lens as described in Eq. (3.1.2) by just being rotated. Even though Gaussian Schell beams are not transversally truncated paraxial beams and the propagation through a lens voids the characteristics of a Gaussian Schell beam, the Wigner function can still be used to describe the beam after passing through a lens or an aperture.

### 3.2 Characterization of general partially coherent beams

The beam quality is a fundamental characteristic when lasers with high power output are designed for the industry. High laser power is dependant on a well focussed beam and a high degree of far-field angular convergence while inhomogenities in the gas flow can severely degrade the beam quality and therefore lower the power output[2]. Potential problems like these complicate the search for a general characterization of laser beams that is valid for any arbitrary beam where the possibilities of explicit, analytical or numerical calculations exist and are directly measurable. Partially coherent Gaussian Schell beams satisfy these characteristics and provide a major advantage seeing that they also can be used in ABCD matrix optics for non-diffractional optical systems.

The in Sect. 2.3 introduced second-order moments of the Wigner distribution function can be utilized to express the quality parameter $Q_{x/y}$ in bidimensional optical systems for position $r_{x/y}$ and direction $u_{x/y}$. Such bidimensional systems have cylindrical symmetry and symmetric beams where the beam quality is calculated by

$$Q_x = \langle r_x^2 \rangle \langle u_x^2 \rangle - \langle r_x u_x \rangle^2 \tag{3.2.1}$$

The waist diameter $D_{x/y}$ and divergence angle $\theta_{x/y}$ of a beam can be substituted by the presented Wigner Moments:

$$D_x = 4\sqrt{\langle r_x^2 \rangle} \tag{3.2.2}$$

$$\theta_x = 4\sqrt{\langle u_x^2 \rangle} \tag{3.2.3}$$

Because of the symmetry of the beam in the bidimensional system, $D$ and $\theta$ are each the same in both $x$ and $y$ direction. These may be implemented in $M^2$ to allow the computation of the beam quality in bidimensional sysytems at any given point on the beam[1]:

$$M_x^2 = \frac{D_x \theta_x}{4} \frac{\pi}{\lambda} = \frac{4\pi}{\lambda} \sqrt{\langle r_x^2 \rangle \langle u_x^2 \rangle - \langle r_x u_x \rangle^2} \tag{3.2.4}$$

$Q$ and $M$ can be defined for every plane $z$ implying the equation is legit everywhere in the beam and fulfills the following uncertainty principle

$$Q \geq \frac{1}{4} k^2, \qquad k = \frac{2\pi}{\lambda} \tag{3.2.5}$$

while $M_x^2 \geq 1$.
$Q_y$, $D_y$, $\theta_y$ and $M_y^2$ are calculated analogous to their $x$ counterparts.

The convenience of these definitions lie in their simplicity by describing the spatial and angular widths of a beam as a function of its coherent properties, while depending on the invariance of the quality parameter under propagation through ABCD systems. In reality however, beams are not cylindrical symmetric, meaning $Q$ and $M^2$ would stay constant for the entire propagation of the beam. For the reason that an aperture or lens would change the beams properties, an extension to tridimensional optical systems has to be made. In order to generalize this notation, the Wigner distribution function will be extended for tridimensional optical systems to $W(r_x, r_y, u_x, u_y, z)$ where $r_x$ and $r_y$ denote the position, $u$ the angular direction for each the $x$ and $y$ direction and $z$ the optical axis. The beam quality for three dimensional systems emerges as

$$Q_{3D} = \langle \boldsymbol{r}^2 \rangle \langle \boldsymbol{u}^2 \rangle - \langle \boldsymbol{r}\boldsymbol{u} \rangle^2 = (\langle r_x^2 \rangle + \langle r_y^2 \rangle)(\langle u_x^2 \rangle + \langle u_y^2 \rangle) - (\langle r_x u_x \rangle + \langle r_y u_y \rangle)^2 \tag{3.2.6}$$

while $\boldsymbol{r}$ and $\boldsymbol{u}$ are the vectors containing their seperate coordinates $r_{x/y}$ and $u_{x/y}$. Even though this applies for any arbitrary tridimensional beam, it cannot straightforwardly be used when a beam propagates through e.g. a lens or is reflected at a mirror since it can completely change the direction. If this is the case, all planes of observation have to be rotated to face the right direction.
First, the tridimensional beam can be transferred into the beam matrix $P$:

$$\boldsymbol{P} = \begin{bmatrix} \boldsymbol{W}^2 & \boldsymbol{\Psi} \\ \boldsymbol{\Psi}^T & \boldsymbol{\Phi}^2 \end{bmatrix} = \begin{bmatrix} \langle r_x^2 \rangle & \langle r_x r_y \rangle & \langle r_x u_x \rangle & \langle r_x u_y \rangle \\ \langle r_x r_y \rangle & \langle r_y^2 \rangle & \langle r_y u_x \rangle & \langle r_y u_y \rangle \\ \langle r_x u_x \rangle & \langle r_y u_x \rangle & \langle u_x^2 \rangle & \langle u_x u_y \rangle \\ \langle r_x u_y \rangle & \langle r_y u_y \rangle & \langle u_x u_y \rangle & \langle u_y^2 \rangle \end{bmatrix} \tag{3.2.7}$$

The sub-matrices $\boldsymbol{W}$, $\boldsymbol{\Psi}$ and $\boldsymbol{\Phi}$ are defined as

$$\boldsymbol{W}^2 = \begin{bmatrix} \langle r_x^2 \rangle & \langle r_x r_y \rangle \\ \langle r_x r_y \rangle & \langle r_y^2 \rangle \end{bmatrix}, \quad \boldsymbol{\Psi} = \begin{bmatrix} \langle r_x u_x \rangle & \langle r_x u_y \rangle \\ \langle r_y u_x \rangle & \langle r_y u_y \rangle \end{bmatrix}, \quad \boldsymbol{\Phi}^2 = \begin{bmatrix} \langle u_x^2 \rangle & \langle u_x u_y \rangle \\ \langle u_x u_y \rangle & \langle u_y^2 \rangle \end{bmatrix}. \tag{3.2.8}$$

$P$ can be transformed to represent the output of the ABCD optical system as beam matrix $P'$ where the optical system is portrayed by the 4x4 matrix $M$:

$$\boldsymbol{P'} = \boldsymbol{M}\boldsymbol{P}\boldsymbol{M}^T \tag{3.2.9}$$

The rotation of the planes is achieved by making use of the Wigner Moments to compute the rotation matrix $G_\beta$ of the $ABCD$ system which can then be reduced to express the angle of rotation $\beta$:

$$G_\beta = \begin{bmatrix} cos(\beta) & sin(\beta) & 0 & 0 \\ -sin(\beta) & cos(\beta) & 0 & 0 \\ 0 & 0 & cos(\beta) & sin(\beta) \\ 0 & 0 & -sin(\beta) & cos(\beta) \end{bmatrix} \tag{3.2.10}$$

$$cot(2\beta) = 2\frac{\langle u_x u_y \rangle}{\langle u_y^2 \rangle - \langle u_x^2 \rangle} \tag{3.2.11}$$

## 4 Implementation into a raytracing framework

In previous chapters, the modelling of light as a ray has been mathematically explained. Now the general steps on implementing Gaussian Schell beams into a raytracing framework will be laid out and finally an evaluation of the presented model will be shown. The model will allow the display of collections of beams as e.g. a laser beam. With the help of the underlying raytracing framework, such beam can be propagated through optical systems containing lenses or mirrors whereas the evaluation will be solely done for single Lens systems.

### 4.1 Generating Wigner distributed rays

At first the Wigner distributed rays (from now on referred to as Wigner rays) have to be created. In the example of Fig. 5, such a beams cross-section is visualized by the outer circle. The beam itself is split up into 2 azimuthal rings with 5 and 10 individual rays evenly spread on each ring. Every single one of these rays is going to be discretized as Eq. (4.1.1) suggests. Such cluster of rays in a beam will be called ray space or Wigner ray space if the rays are discretized and the Wigner distribution is considered. For this purpose, a grid with size $n \times m$ $(n, m > 0)$ will be constructed with rays being sent in each direction $(i, j)$ (in the right hand grid of Fig. 5) with position $\boldsymbol{r}$ (in the left hand grid of Fig. 5). $\boldsymbol{r}$ is a 3-dimensional vector as $\boldsymbol{r} = (r_x, r_y, r_z)^T$ for each separate ray while $r_z$ is constant for one plane of observation. Here, $\boldsymbol{r}$ can be derived by discretizing the exponential term $\exp(-\frac{2\boldsymbol{r}^2}{w^2(z)})$ of the Wigner distribution function in Eq. (3.1.2) for each ray in the beam. The direction $\boldsymbol{u}$ however has to be computed by using a discretization for each point in the grid of every single ray in the ray space (see right hand side of Fig. 5):

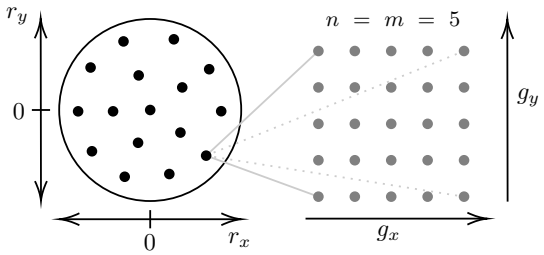


Fig. 5: Visualization of the discretization of an individual ray in a beam with 2 azimuthal rings with 5 and 10 rays per ring (left hand side) while each ray is discretized in a $5 \times 5$ grid (right hand side)

$$g_x = u_{x_{min}} + i\frac{u_{x_{max}} - u_{x_{min}}}{n-1}, \qquad g_y = u_{y_{min}} + j\frac{u_{y_{max}} - u_{y_{min}}}{m-1} \tag{4.1.1}$$

The minimum and maximum value for $g$ are derived from the last exponential equation in Eq. (3.1.2) since it embodies the position and direction of the ray. To achieve this, $\exp(-\frac{2}{\theta}(\frac{r}{R}^2))$ is solved for $e^{-t}$. In this case, $t = 2$ is used as it may generally be utilized as the threshold of the intensity needed to measure the beam's diameter:

$$\begin{aligned} e^{-\frac{2}{\theta^2}\cdot(\boldsymbol{u}-\frac{\boldsymbol{r}}{R})^2} &= e^{-2} \\ -\frac{2}{\theta^2}\cdot\left(\boldsymbol{u}-\frac{\boldsymbol{r}}{R}\right)^2 &= -2 \\ (u_{x_{min/max}} - \frac{r_x}{R})^2 + (u_{y_{min/max}} - \frac{r_y}{R})^2 - \theta^2 &= 0 \end{aligned} \tag{4.1.2}$$

$u_{y_{min/max}}$ has to be set to zero in order to get to the equation for $u_{x_{min/max}}$ and vice versa. The result can be solved by the quadratic formula to:

$$u_{x_{min/max}} = \frac{r_x}{R} \mp \sqrt{\theta^2 - \left(\frac{r_y}{R}\right)^2} \tag{4.1.3}$$

The calculation of $g_y$ and $u_{y_{min/max}}$ is analogous while $\theta^2$ is simply expressed by

$$\theta^2 = \frac{\lambda^2}{\pi^2 w_0^2} \tag{4.1.4}$$

The tangent of $g$ finally provides the components for the normalized direction vector of the ray:

$$\mathbf{u}_{ray} = \begin{pmatrix} tan(g_x) \\ tan(g_y) \\ \sqrt{1 - tan(g_x) - tan(g_y)} \end{pmatrix} \tag{4.1.5}$$

The intensity for each discretized beam in the grid is simply given by the Wigner function (Eq. (3.1.2)) while the intensity $I_0$, the beam radius $w(z)$ and degree of coherence $\beta$ are specified in the input. $L_c$ is computed by altering Eq. (3.3):

$$L_c = \frac{w_0}{\sqrt{\frac{1}{\beta^2} - 1}} \tag{4.1.6}$$

Algorithm 1 demonstrates an abstract guideline to the implementation of the Wigner intensity for each ray in the existing ray space. At first a ray space has to be created for all rays in the beam. Then the iteration for all rays begins while an inner loop iterates over all points in the discretized $u_x, u_y$ grid. Here, each Wigner ray is discretized, then its direction computed and the Wigner intensity calculated. Finally, the created Wigner ray is added to the existing Wigner ray space and the next ray is going to be covered.
Thanks to the Wigner rays simply being an enhancement in terms of the intensity of the standard rays, further propagation through optical systems can be handled by the existing raytracing framework without any modifications.
It is worth to note that the size of the discretization grid can only be chosen to such extent, that the original beam does not exceed the maximum diameter to pass e.g. a lens. This is due to the fact that a larger grid size increases the general beam diameter.

**Algorithm 1** Generate Wigner rays in a ray space

```
1: function createWignerRays(raySpace)
2:     wignerRaySpace =new raySpace()
3:     for each Ray ray in raySpace do
4:         for each position p in discretizedGrid do
5:             g = discretize(p)
6:             ray.u = getDirection(g)
7:             ray.intensity = wignerIntensity(ray.r, ray.u)
8:             wignerRaySpace.append(ray)
9:         end for
10:    end for
11:    return wignerRaySpace
12: end function
```

### 4.2 Wigner moments and beam quality

Characterizations of beam properties and their mathematical descriptions have been introduced in Sect. 2.3 and Sect. 3.2. As mentioned the implementation of the beam quality $Q_{3D}$ requires the planes of observation to be facing the $z$-direction. This rotation of the current wave field, is done by rotating every beam by the angle $\beta$. Once this is done can the Wigner moments be calculated whereas the equation is changed to compute the integral with the help of numerical integration as a sum for the $x$ and $y$ coordinates of every point $\boldsymbol{r}$, its direction $\boldsymbol{u}$ and individual power $p_i$ [1]. Because of small intensities $I$ outside the observed beam can the following approximation be used for the Wigner moments:

$$\langle r_x^2 \rangle = \frac{1}{P} \int\int r_x^2 \cdot W'(\boldsymbol{r}, \boldsymbol{u})\, d\boldsymbol{r} d\boldsymbol{u} = \frac{1}{P} \int r_x^2 I(\boldsymbol{r})\, d\boldsymbol{r} \approx \frac{1}{P} \sum_i p_i x_i^2 \tag{4.2.1}$$

$$\langle r_x u_x \rangle = \frac{1}{P} \int \int r_x u_x \cdot W'(\boldsymbol{r}, \boldsymbol{u})\, d\boldsymbol{r} d\boldsymbol{u} \approx \frac{1}{P} \sum_i p_i r_{x_i} u_{x_i} \tag{4.2.2}$$

Once all required moments are known can the tridimensional beam quality $Q_{3D}$ be evaluated by using Eq. (3.2.10) and the proposed functions in form of

**Algorithm 2** Compute the beam quality $Q_{3D}$ for wigner distributed beams

```
1: function EVALUATEWIGNERRAYS(wignerRaySpace)
2:     rotatePlanes(wignerRaySpace)
3:     wignerMoments = calculateWignerMoments()
4:     Q_3D calculateQ_3D(wignerMoments)
5:
6: end function
```

### 4.3 Limitations of the Wigner distribution function

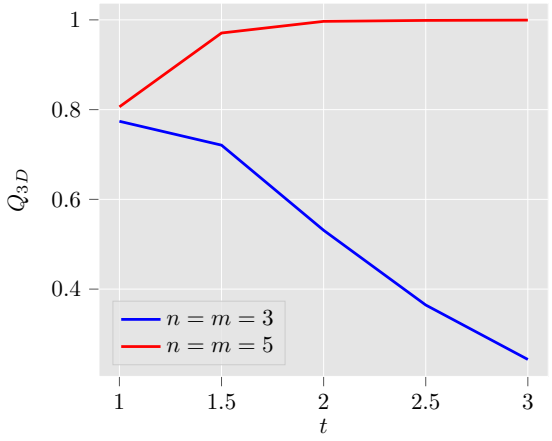


Fig. 6: Plot of the beam quality (at the source) over increasing values for $n = m$ with initial beam radius $w = 4\,\text{mm}$

The radius of a beam of light is dependant on the radius where its intensity drops to a certain threshold $e^{-t}$. The larger the value of $t$, the bigger the radius and the more rays can be discretized. More rays and a finer grid allow a more precise computation of the beam quality which means that $t, n$ and $m$ should be as large as possible. Fig. 6 visualizes the accuracy of the computation of the beam quality. A sparsely discretized grid with $n = m = 3$ shows strong deviation from an ideal $Q_{3D} = 1$ at the source and even decreases for larger $t$. Meanwhile, $Q_{3D}$ quickly converges towards 1 with $n = m = 5$. Following this observation, a minimum of $n = m = 5$ and $t = 2.0$ may be used to calculate the beam quality $Q_{3D}$. In an optical system containing a single lens, the limiting factor for $t$ is the radius of the lens. If $t$ is choosen in such a way that the beam radius exceeds the radius of the lens, no viable results are achievable. Eq. (4.1.2) has been solved with $t = 2$ as a relatively high accuracy is achieved. Experiments have shown that for a grid of size $n = m = 5$, the maximum beam radius should be $w < 10\,\text{mm}$ for all rays to fit through a lens with a radius of 12.7 mm .

### 4.4 Evaluation

Lastly, the implemented formulas need to be evaluated by comparing the simulated results to the experimental results from [5]. The code is run for several different initial spot sizes ranging from 1 to 9 mm in radius. In the experiment of [5], a 633 nm He-Ne laser operating in the $TEM_{00}$ mode is propagated through a thin uncorrected plano-convex lens where the convex side is oriented towards

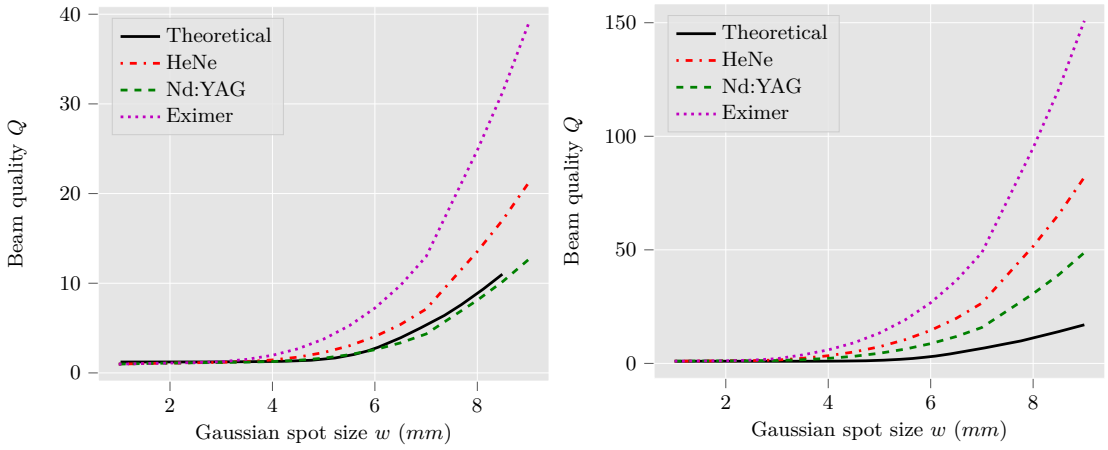


Fig. 7: The lasers used in this experiment emit the following wavelengths: Nd:YAG laser at 1 064 nm, HeNe laser at 633 nm and the eximer laser at 344 nm. The solid line displays the solutions of the theoretical expressions for a HeNe laser [5] and a plano-convex lens with the convex side oriented towards the source was used in a) and the other way around in b).

the source. In the simulation, the laser beams are sent through an optical system consisting of a plano-convex lens with a radius of curvature of 45 mm. The lens is situated 25 mm away from the source while the convex site is oriented towards the starting plane in Fig. 7a and the other way around in Fig. 7b. The mostly collimated beam will be focussed by the lens and evaluated at the final plane of observation 100 mm away from the lens. Fig. 7 shows the measured and theoretical beam qualities as a function of the Gaussian spot size $w$. The measurements slightly deviate from the theoretical beam quality in the range of $w \approx w_q$, where $w_q$ is the beam radius at the lens. At this point the spherical abberations are beginning to take effect which in [5] was proposed to be the consequence of interactions between the aberrating effects of the plano-convex lens and similar effects in the microscope objective. Since there is no microscope to be the source of this, the actual reason for the drift is explained by the praxial approximations to Snell's law used in deriving the equations[5]. The rather extreme difference in beam quality between the two orientations of the lens, may originate from the different diffractions at the surfaces of the lenses. In contrast to the curved side of the lens being oriented towards the source, the rotated orientation shows less diffraction at larger angles and thus stronger potential aberration resulting in a higher value for $M^2$. While **??** only shows the theoretical beam quality for a Helium-Neon laser, the same applies for the other wavelengths. Here it is worth noting that smaller wavelengths usually result in smaller divergence angles and thus more collimated beams. Even though this is true, the beam quality in Fig. 7a decreases on smaller wavelengths. The reasaon for this is that phase errors and aberration effects are increasingly produced for smaller wavelengths. Combined with the increased abberation from diffraction, $M^2$ shows an even faster growth in the reverse orientation of Fig. 7b.

## 5 Conclusion

Regardless of the in the previous chapter stated imprecision, the Gaussian Schell model will be a well founded addition to the developed framework as it will help determine important beam

properties such as the implemented beam quality. As the bidimensional beam quality may only be used in symmetrical optical systems for cylindric symmetrical beams, the tridimensional beam quality has been introduced. This can be used for any arbitrary Gaussian Schell beam in non-symmetric optical systems. Moreover, it can relatively straightforward be implemented as demonstrated in Sect. 4.1 and the in Sect. 4.4 shown results underline the convenience of this approach. Potential problems such as negative frequencies may even become advantages since negative frequencies and thus negative values for the Wigner distribution function simply indicate interfering Gaussian Schell beams.

## References

1. Eppich, B.: Design of optical systems for laser radiation based on local second order moments and gauss-schell ray bundles (2018)
2. J. Serna, R. Martinez-Herrero, P. M. Mejias: Parametric characterization of general partially coherent beams propagating through abcd optical systems (7 July 1991)
3. Luecking, S.: dürer, drawing, and digital thinking. `http://www.brian-curtis.com/text/conferpape_steveluecking.html` (Accessed: 07 June 2021)
4. Max Born, Emil Wolf: Principles of optics, 6th edition. Pergamon Press Ltd. (1980)
5. Siegman, A.E.: Analysis of laser beam quality degradation caused by quartic phase aberrations (20 October 1993)
6. University of California, Physics Department: Properties of helium-neon lasers (2006)
7. Wolfgang Singer, Michael Totzeck, Herbert Gross (ed.): Handbook of Optical Systems, Volume 2: Physical Image Formation (May 2006)